

Chapter 2

Description of the Zn/Br RFB System

Abstract In order to make beneficial changes to the Zn/Br flow battery system, it is necessary first to understand its present structure and functional status, including the level of performance for typical systems, the operating mechanisms as well as the conventional materials and methods of construction. The previous chapter introduced and discussed the need for reliable large-scale electrical energy storage and the role of redox flow batteries for such purposes. This chapter describes the physical architecture of the Zn/Br system (i.e. electrode stack, membrane separator, electrolyte flow schematic), as well as the conventional electrolyte solution employed and the dominant chemical redox reactions occurring during charge and discharge processes at each electrode. Design considerations are detailed, such as the safe storage and treatment of bromine evolved, together with important operating practices such as tracking state-of-charge. Finally, electrochemical and overall operational performance characteristics are discussed with regard to maximizing the specific energy of the Zn/Br flow battery and scaling-up next-generation systems from benchtop testing to commercial use.

2.1 Physical Architecture

The Zn/Br redox flow battery (RFB) is a modular system comprising a cell stack containing functional electrodes attached to current collectors (separated via membranes), electrolyte storage tanks/reservoirs, delivery pumps and pipes. The RFB relies on the electrolyte circulation system to deliver electrochemically active species to electrode surfaces in order to achieve charge transfer and cause electrical current to flow. A simple Zn/Br unit cell is illustrated in Fig. 2.1, with multiple such cells combined in series to create a practical battery.

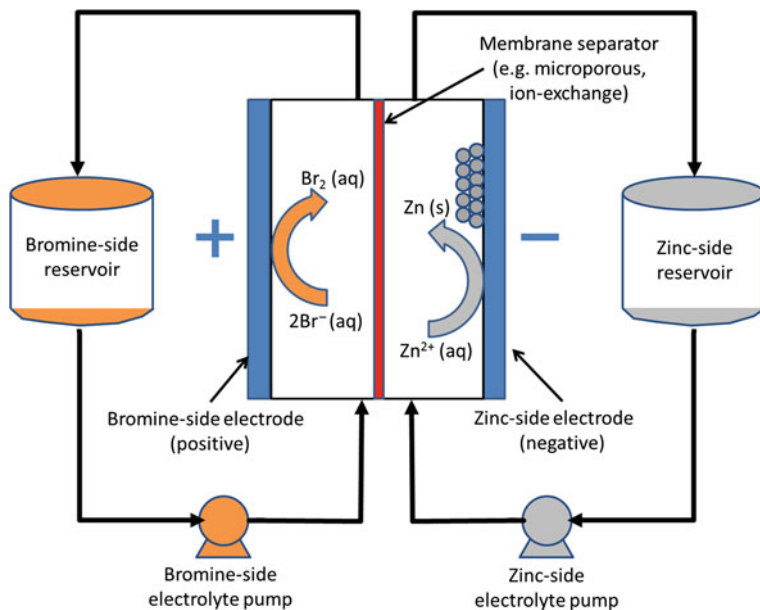


Fig. 2.1 A simple Zn/Br unit cell (with electrolyte reservoirs and pumps) during charging process, with positively polarized bromine-side and negatively polarized zinc-side electrodes

2.2 Electrolyte Composition

The main electrolyte used in zinc/bromine batteries (ZBBs) is zinc bromide (ZnBr_2) dissolved in water to form an aqueous solution, with the same formulation being used in circulatory loops servicing both the cathode and anode during operation. ZnBr_2 is the primary electrochemically active species that interacts with the electrodes to participate in charge-transfer reactions that allow the system to function as an energy storage device. The ZnBr_2 present is typically of high concentration, ranging between 1 and 3 M [1], with the possibility of even higher concentration up to 4 M [2]. Significant variation in this amount is a direct result of the stage of the charge/discharge cycle at which the battery is, with the concentration decreasing significantly as charging progresses and Zn^{2+} is plated-out while Br^- is oxidized to Br_2 , then climbing back up again as the battery is discharged and the original ZnBr_2 concentration is restored.

A potential-pH (Pourbaix) diagram for a 2.5 M ZnBr_2 primary electrolyte solution was constructed using OLI Studio software (version 9.2, OLI Systems, Inc.) and is presented in Fig. 2.2.

The evolution of bromine from bromide anions during charging is an important process in ZBB operation. Due to the toxic and corrosive nature of bromine, a complexing agent is added to the electrolyte to sequester bromine into an alternate phase with low vapor pressure. This sequestration prevents bromine escaping from

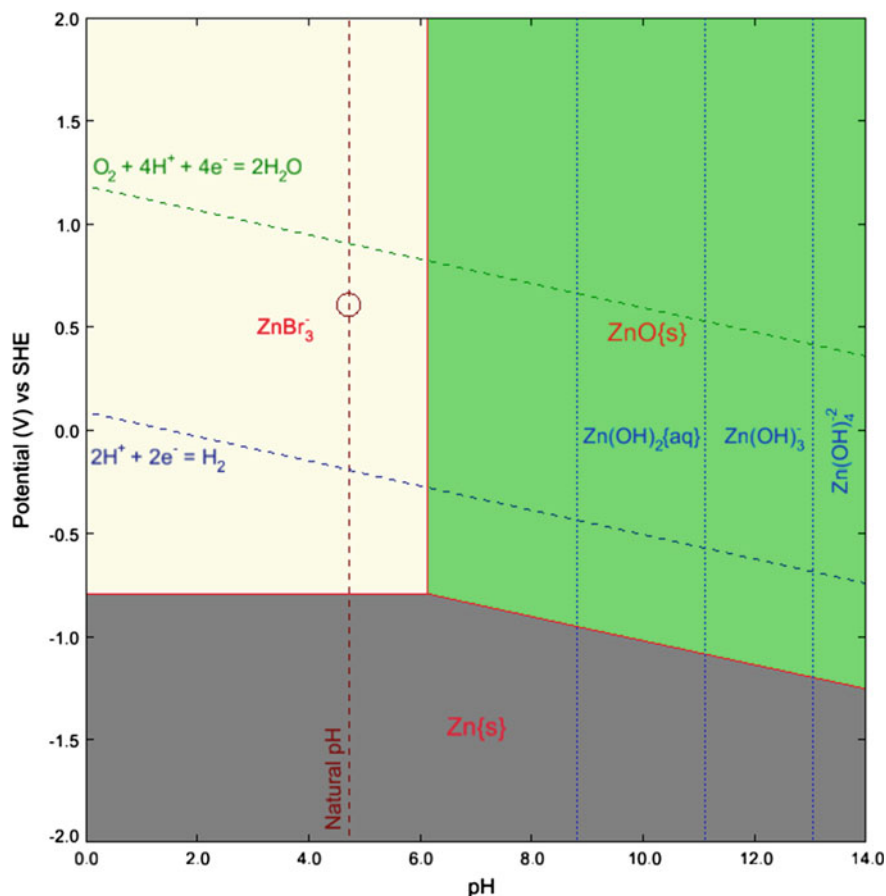


Fig. 2.2 Pourbaix diagram (potential vs. pH) of a 2.5 M ZnBr_2 electrolyte solution, indicating stability regions of various Zn-based predominant species (The various speciation stabilities of Zn were calculated using the Margules ion exchange model at standard conditions of 25 °C and 1 atm across a pH range of 0–14 (adjusted using HBr and KOH) between potentials of –2 and 2 V versus standard hydrogen electrode (SHE). The “AQ (H^+ ion)” thermodynamic framework present within OLI Studio was utilized and redox chemistry calculations were included for all subsystems present. The stability regions for different Zn-based species and their phases are indicated on the diagram, with solid lines representing solid phases and dotted lines indicating aqueous phases. The natural pH of the electrolyte is also indicated on the figure, as well as aqueous lines indicating the evolution of hydrogen and reduction of oxygen. (together with the relevant equations))

solution as a vapor and interacting with the system’s environment in its elemental form. The bromine that evolves is typically complexed with a quaternary bromide salt (QBr) such as N-methyl N-ethyl pyrrolidinium bromide (MEP) or N-methyl N-ethyl morpholinium bromide (MEM) [3], which are illustrated in Fig. 2.3 (on the left and right, respectively).

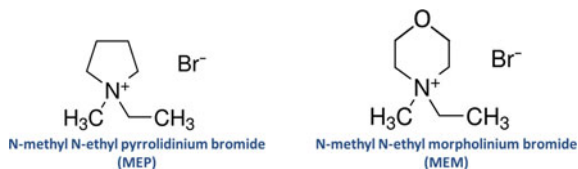


Fig. 2.3 Structures of the N-methyl N-ethyl pyrrolidinium bromide (MEP, *left*) and N-methyl N-ethyl morpholinium bromide (MEM, *right*) ionic liquids conventionally used to sequester bromine during the Zn/Br RFB charging process

The sequestered elemental bromine is stored safely in an oily phase that remains separate from the main aqueous electrolyte due to the higher specific gravity of the sequestered phase. The concentration ratio of QBr to ZnBr₂ generally employed is approximately 1:3 [1, 4], hence a 3 M ZnBr₂ electrolyte solution could typically contain 1 M of bromine sequestering agent (BSA). Effective sequestration can result in bromine concentrations in the main electrolyte falling to values as low as 0.1 M [2]. Other solvents such as propionitrile [5–7] have also been tested but have exhibited lower conductivity and higher toxicity and flammability [8], giving rise to the popularity of QBr compounds as the preferred alternative for bromine sequestration in Zn/Br systems. However, concerns regarding the compatibility of MEM and MEP with various bromide reactions have prompted recent work to find suitable alternatives [9].

Figure 2.4 shows a possible 3D molecular arrangement of gas-phase MEPBr and two sequestered Br₂ molecules. The structure is optimized by carrying out

Fig. 2.4 Possible structure (optimized via periodic density functional calculations) of MEPBr and two sequestered Br₂ molecules, with the color convention for atoms: *black* for carbon, *grey* for hydrogen, *red* for nitrogen and *blue* for bromine

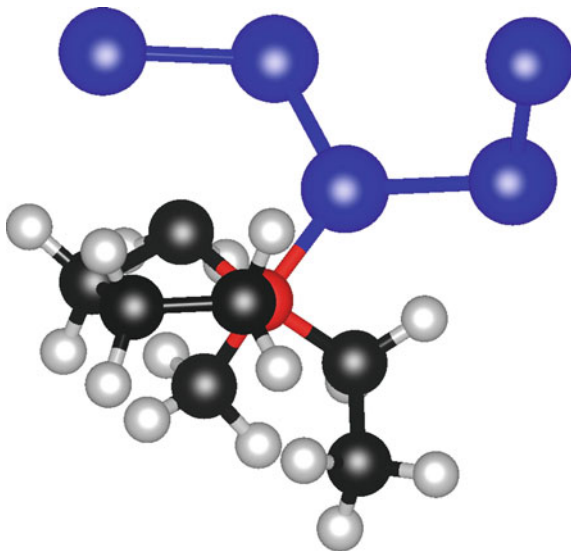
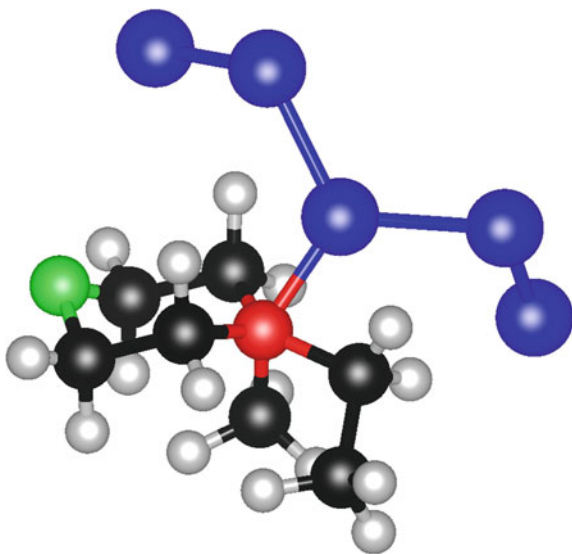


Fig. 2.5 Possible structure (optimized via periodic density functional calculations) of MEMBr and two sequestered Br₂ molecules, with the color convention for atoms: *black* for carbon, *grey* for hydrogen, *red* for nitrogen, *blue* for bromine and *green* for oxygen



first-principles periodic density functional calculations using projector-augmented wave (PAW) potentials [10, 11] for describing electron–ion interactions, within the Vienna Ab initio Simulation Package (VASP) software [12].

Figure 2.5 shows a possible 3D molecular arrangement of gas-phase MEMBr and two sequestered Br₂ molecules, using density functional calculations similar to those used for MEPBr with two Br₂ in Fig. 2.4.

It is vital that a well-controlled narrow pH range between 1 and 3.5 is maintained during ZBB operation. Zinc deposits with a moss-like appearance [2, 13] can be observed with weakly acidic and basic electrolytes, whereas more acidic environments cause significant gaseous hydrogen evolution [2] that would in turn expedite zinc corrosion. Consequently, significant drops in coulombic efficiency can be expected on deviation from this working pH range due to charge being lost when protons are converted to H₂ gas instead of through the primary charge carriers of the battery.

It is common practice to introduce other electrochemically active species to boost operating efficiency and ionic activity by increasing the electrolyte’s conductivity. An important implication to consider when introducing any type of additive is the corresponding increase in the weight of electrolyte present in the ZBB unit. Unless the compound is highly effective in increasing the electrochemical efficiency of important processes, it could negatively influence the specific energy of the system and raise production costs.

Common supporting additives include potassium chloride and ammonium-based chlorides and bromides [8, 14]. These secondary electrolytes are usually added in smaller quantities than the main electrolyte and should be neutral salts in order to

avoid undesirable changes to the acidic electrolyte's working pH range [1]. The type of additive used can influence the behavior of the system. For instance, zinc electrowinning from zinc chloride baths has been found to produce rough and porous deposits [15].

A Pourbaix diagram for a 2.5 M ZnBr_2 primary electrolyte solution containing 0.9 M ZnCl_2 as a supporting electrolyte was constructed and is presented in Fig. 2.6 using a methodology similar to the calculation for pure ZnBr_2 presented in Fig. 2.2. Interestingly, there appears to be no significant change in the dominant Zn-based species, with only slight shifts in the natural pH (becoming slightly more acidic) and the vertical pH lines (slightly more basic) separating different ionic species.

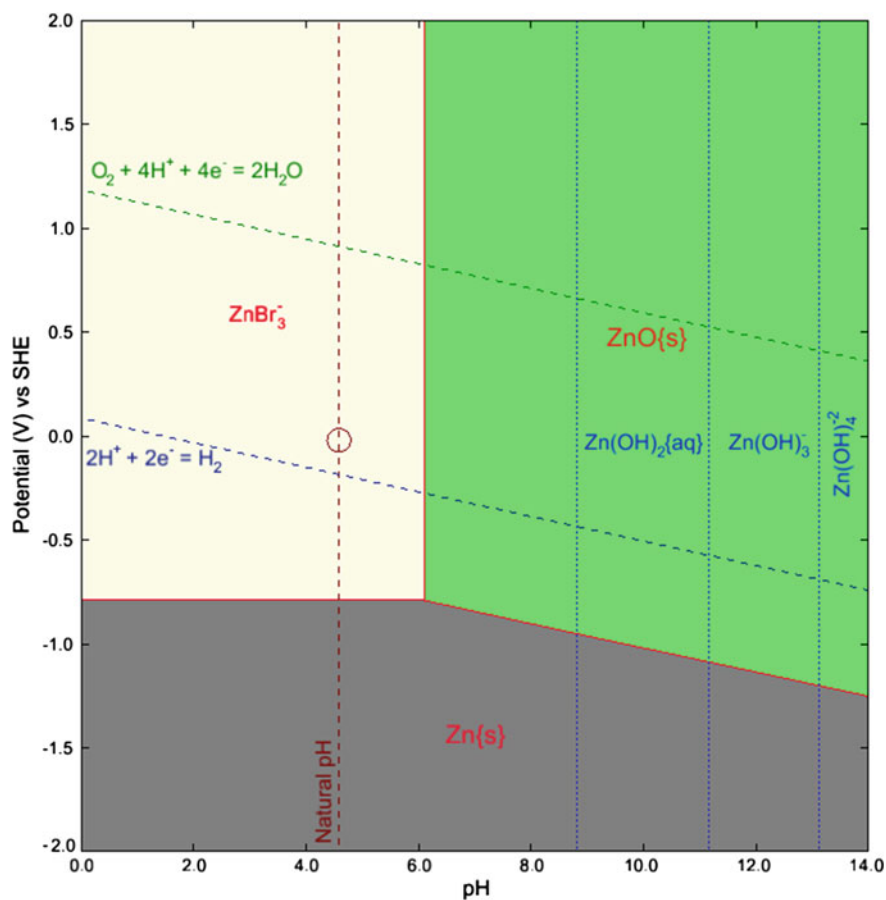


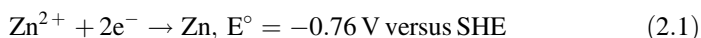
Fig. 2.6 Pourbaix diagram (potential vs. pH) of a solution containing 2.5 M ZnBr_2 (primary electrolyte) and 0.9 M ZnCl_2 (secondary electrolyte), indicating stability regions of various Zn-based predominant species

2.3 Zn/Br Electrode Reactions

Electrodes used in ZBB cell stacks are bipolar, where a single electrode has a “positive” and “negative” side. Materials of construction for these electrodes include metals and carbon-plastic composites.

2.3.1 The Zinc-Side Electrode

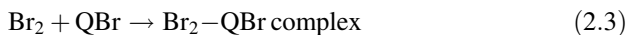
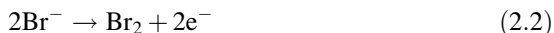
In essence, the zinc half-cell of the ZBB behaves very similarly to an electroplating system. During the charging process, cationic zinc comes out of the aqueous solution to be electroplated onto the negative side of the bipolar electrode in the cell stack [8], as shown by Eq. 2.1:



The reverse occurs during discharge of the battery as the electroplated zinc loses two electrons to the bipolar electrode and dissolves back into aqueous solution.

2.3.2 The Bromine-Side Electrode

During charging, bromide anions are converted to bromine which is subsequently complexed with a QBr and stored safely as a separate liquid phase [1], as shown by Eqs. 2.2 and 2.3:

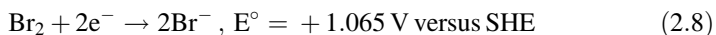
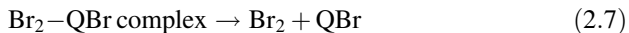


The QBr-polybromide complex is removed from the vicinity of the electrode surface by constant circulation of the electrolyte within the battery (via pumps) during the charging process. Similarly, electrolyte circulation is used to transport the complex from storage within the tanks/reservoirs to the electrode surface for charge transfer to occur. Additionally, monobromide ions have been found to react with aqueous bromine being evolved during charging to form tribromide ions and higher polybromides [16, 17], as shown by Eqs. 2.4–2.6:





During discharge, bromine dissociates from the QBr complex and is reduced to the anionic bromide form, as shown by Eqs. 2.7 and 2.8:

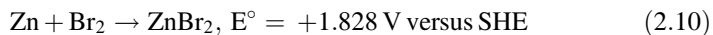


2.3.3 Overall Battery Reaction

When the ZBB is charged, the overall chemical reaction involves the reduction of zinc and evolution of bromine, as shown by Eq. 2.9:



Similarly, zinc and bromine recombine to form ZnBr_2 when the ZBB is discharged, as shown by Eq. 2.10:



Based on the individual half-cell reaction potentials, the theoretical electrochemical potential offered by a single Zn/Br cell should be approximately 1.828 V. This value is the Nernstian potential under zero current flow. However, the presence of internal inefficiencies and various resistance contributions seen in practice are expected to result in slightly lower cell voltage values. Another important performance metric for Zn/Br systems is current density, which is the amount of current passing through a unit area of an electrode surface. The current density, in turn, has a direct influence on the electrode capacity (i.e. energy per unit area) as well as the operating efficiency of the overall system.

An example of how battery voltage and current within a bench-scale Zn/Br system change during full-cell charge/discharge cycling is presented in Fig. 2.7. This curve was obtained from 2 h of charging followed by 2 h of discharge phase under a current density of 20 mA cm^{-2} using graphite-coated carbon nanotube-embedded high-density polyethylene electrodes and a battery solution comprising 2.5 M ZnBr_2 primary electrolyte and 1 M MEP.

An example of how the energy balance and total capacity of the Zn/Br battery in Fig. 2.7 change during charge/discharge cycling is presented in Fig. 2.8.

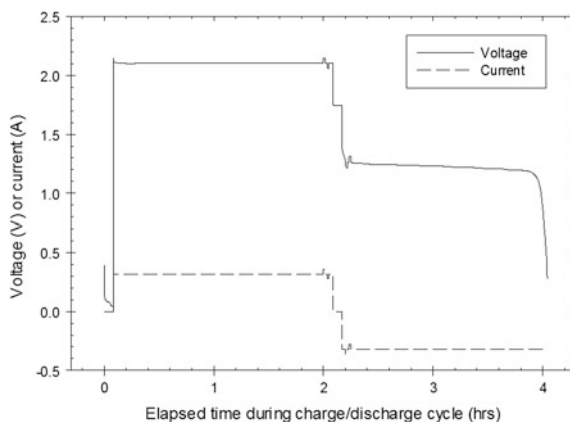


Fig. 2.7 Profiles of transient battery voltage and current during full-cell charge/discharge cycling of a bench-scale Zn/Br system (*Experimental data kindly provided by Martin Schneider of the Energy Storage Group at the University of Sydney.*)

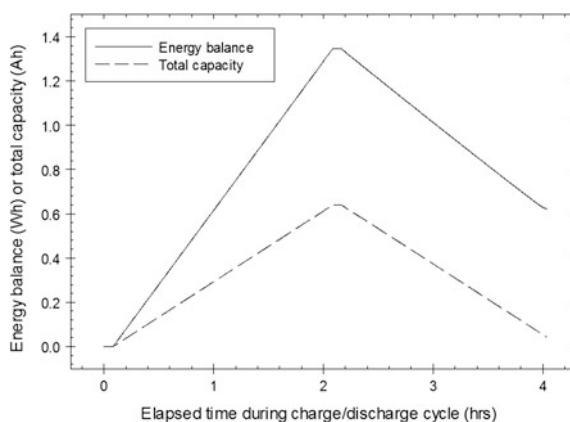


Fig. 2.8 Profiles of transient energy balance and total capacity during full-cell charge/discharge cycling of a bench-scale Zn/Br system (*Experimental data kindly provided by Martin Schneider of the Energy Storage Group at the University of Sydney.*)

2.4 Bromine Storage, Treatment and Toxicity

Depending on the state-of-charge (SoC) during the charge/discharge cycle of the ZBB, bromine exists in various forms within the electrolyte solution: as elemental bromine upon charging (i.e. Br_2), monobromide, tribromide, pentabromide or higher. Of these, aqueous elemental bromine is volatile and risks escaping into the external environment as a gas in the event of containment breaching. This is avoided by sequestering the Br_2 into a complex liquid phase using a suitable QBr,

thereby lowering its vapor pressure and likelihood of escape. Information about bromine toxicity is readily available in material safety data sheets [18]. Contact with gaseous elemental bromine is hazardous to health as it is damaging to the eyes and skin. It is detectable by its strong suffocating odor and can be fatal if inhaled as it damages the respiratory system. Bromine is also harmful to the environment, especially to aquatic life. Consequently, the safe operation of Zn/Br RFBs is an important factor influencing the uptake of the technology for utility-scale electrical energy storage.

2.5 Membrane Separator

The membrane separator is an integral component in the Zn/Br RFB as it serves as a barrier that prevents cross-contamination of electrochemically active species in the system, as well as reducing possible electrical contact across electrodes. An electrochemical requirement of the system is to minimize the diffusion of Br_2 to electroplated Zn as much as reasonably possible, to prevent self-discharge of the ZBB when it is charged but left unused for an extended period of time. The occurrence of self-discharge would in turn lead to lower coulombic efficiency of the system. This self-discharge mechanism is attributed to the action of aqueous bromine evolved on the bromine side migrating to the zinc-side electrode and subsequently oxidizing the electroplated zinc, thus causing the battery to discharge itself [19]. Thermodynamically, bromine is an effective corrosion agent of zinc, indicating the severity of problems faced by the ZBB if the issue is left unchecked [20]. This is avoided by the use of independent circulatory loops for the aqueous zinc bromide electrolyte on both sides of the bipolar electrode stack, together with a microporous film or ion exchange membrane serving as a separator [21].

Two possibilities have been proposed to explain the principles governing bromine diffusion through membranes: it is possible that (a) the action of bromine complexes wetting the separator provides a pathway for elemental bromine to diffuse through or (b) there exists an equilibrium between the bromine in the aqueous phase diffusing through the separator and that in the bulk electrolyte [13]. Studies comparing various ion-exchange membranes have shown that diffusion coefficients of bromine have a wide range of values between 1.44×10^{-10} – $3.74 \times 10^{-10} \text{ cm}^2 \text{ s}^{-1}$ [13] and 1.52×10^{-8} – $2.28 \times 10^{-8} \text{ cm}^2 \text{ s}^{-1}$ [22]. In one set of studies [13], it was also found that the rate of bromine diffusion through the separator in the presence of aqueous and complex phases could be twice as high as that in the presence of an aqueous phase alone.

Due to the nature of bromine diffusion described above, requirements for membrane separators are stringent because a high degree of selectivity is necessary to differentiate between bromide ions and ionic zinc which should be allowed to pass through. The membrane separator also serves as a barrier against the migration of bromine into the zinc-side region, whether in the elemental form or complexed with QBr. As an extension to different interactions with various species, membranes

need to be as chemically inert as possible and not participate in undesirable side-reactions such as promoting degradation of the electrolyte. It is also imperative that membranes used can withstand the harsh operating environment of ZBBs for reasonably extended periods of time. Durability is thus an important factor when selecting the appropriate membrane for use in the system. Various materials with specific properties have been tested for use in ZBBs, including microporous plastic separators such as polyolefin Daramic® [23, 24]. Comparisons between uncoated and fluorine-treated Asahi SF-600 membranes have shown that the latter displayed improved selectivity against bromine diffusion [13]. For the case of plastic-silica composite separators, it has been found that higher silica loading levels result in lower membrane resistivity, consequently contributing towards improved coulombic and energy efficiencies [25].

Stable but more expensive cation-exchange systems such as Nafion® have also been tested [26] and found to be more effective at reducing bromine transport through the separator than their microporous counterparts, because bromide species are mostly present as anionic Br_3^- and Br_5^- complexes [1]. The success of such ion-exchange membranes has prompted a recent review [27] and spurred further work to incorporate multiple such membranes into a single working unit for use in RFBs [28]. Another class of functionalized separators includes sulfonated polysulfone membranes which have been demonstrated as performing better than those constructed via grafting of organic substrates [29].

Membranes constructed from zeolites have also been tested in a vanadium-based system and found to provide a high degree of selectivity based on ion size [30], leading to the transport of desirable species while restricting others. Interestingly, tests carried out in all-V RFBs involving surfactant-functionalized ion-exchange membranes indicate that the amount of water passing through the membrane can be controlled, while also improving overall system performance [31].

Studies of V/Br systems have also found that the ratio of different bromine sequestering agents (MEP and MEM) used in solution have direct influence on voltaic efficiencies due to variation in membrane-related resistances [32]. With motivation from these findings, pursuing similar functionalisation work for Zn/Br RFB membranes as well achieving a suitable balance using mixed BSAs could prove beneficial in the short- to intermediate-term with regard to improved energy efficiencies.

2.6 Accurate Determination of SoC

Determining the SoC accurately and reliably should be considered an integral aspect of ZBB research as it provides a useful pathway towards tracking the degree of impact on battery performance of changes to electrolytes and electrodes. Surprisingly, although SoC is also a clear indicator of whether the full extent of the system's energy storage capacity is being utilized [33], this is a relatively rarely discussed issue in the literature surveyed. Accurate monitoring of SoC is of high

importance and significance as SoC is a direct result of the primary and secondary electrochemical and physical processes occurring within the ZBB as the cyclic charge/discharge operation progresses. With accurate monitoring, therefore, it would be possible to conclusively determine which electrochemically active species cause, dominate and contribute to these processes at any given point in time, thereby indicating which processes might create operational bottlenecks.

A significant proportion of literature pertaining to SoC measurement strategies was published within the past decade, motivated primarily by work carried out on batteries for electric vehicles. Although the open-circuit voltage (OCV) method has been used for ZBBs [34], there are no standard methods in particular. It is increasingly clear, however, that some of the underlying principles and logic might be adapted for use in Zn/Br RFBs regardless of whether the original work was intended for nickel/metal hydride (NiMH), nickel/cadmium (Ni-Cd) or Li-ion systems. Several methods have been developed to measure the SoC of energy storage systems, particularly batteries, including ampere-hour counting, Kalman filters, internal resistance measurement and heuristic techniques based on charge/discharge characteristics [34]. Most direct methods such as OCV and coulometry are too simplistic to robustly handle complex and dynamic systems such as lead/acid batteries [35]. By extension, it can be expected that these methods would pose similar problems in ZBBs due to their relatively complex system configurations.

Relatively recent work on improving the Coulomb counting approach has demonstrated its effectiveness at determining SoC, making it the most convenient method at present [36]. Yet this approach of current integration possesses inherent drawbacks as it does not account for the effects of operating temperature fluctuations or deviations due to operating inefficiencies, hence discharge tests are the only completely reliable means of confirming whether the SoC measurement is correct [37]. This drawback has prompted work to improve the method by applying regular and extended Kalman filters that make corrections for drifts in system behavior [38] and have been proved to be accurate within 2–3 % [39, 40] when estimating SoC in lead/acid batteries. Extended Kalman filters have also been shown to provide good SoC estimations in Li-ion batteries when applied to data obtained via transient cell voltage [41, 42] and OCV [43] measurements. Other direct methods, such as measuring individual half-cell conductivity and tracking changes in electrolyte color during charging or discharging of vanadium RFBs, have also been proved to be simple yet effective strategies [44].

The sensitivity and non-destructive nature of electrochemical impedance spectroscopy (EIS) makes it an attractive method for use in SoC measurement of secondary batteries [45, 46], with the possibility of on-line measurement [34] to avoid disrupting battery operation each time a measurement is required. The benefits of EIS have prompted some successful work involving the modelling of voltage behavior in NiMH batteries based on the concept of impedance [47]. There has also been work to improve fractional system identification in conjunction with Randles' model of lead/acid battery impedance behavior [48], as well as study of the impact of changes in SoC on the linearity of applied current in Li-ion batteries [49]. Voltage drops occurring at the beginning of discharge cycles in lead/acid

batteries have been found to influence the methods and results of SoC calculations [50] and are quite possibly an important phenomenon to keep in view for ZBBs. By extension, it is also necessary to account for other phenomena exhibiting similar behavior (i.e. spikes or drops) upon commencement of charging or discharge of the system, in order to obtain an accurate SoC value.

Adaptive algorithms incorporating hysteresis phenomena have proved effective at estimating SoC in NiMH batteries when calculated using directly obtainable data such as OCV [51]. Comprehensive models have been proposed that account for cycle ageing and temperature effects in Li-ion systems, thereby addressing these requirements for dynamic monitoring of battery performance [52]. It follows that combining these various algorithms could potentially produce highly robust SoC predictions.

The use of artificial neural networks has been shown to be quite effective and computationally efficient in on-line SoC determination for lead/acid [53], NiMH [54] and Li-ion batteries [55]. Independent studies have applied fuzzy logic mathematics to successfully predict SoC in Li-ion batteries [56] as have various systems based on data obtained from Coulomb counting and/or EIS [57]. Self-learning mechanisms incorporating fuzzy neural networks as well as cerebellar-model-articulation and learning controllers are particularly adept at estimating the SoC of systems with nonlinear discharge characteristics [58]. An adaptive neuro-fuzzy inference combination has also been shown to produce fairly reliable SoC estimates [59]. From the numerous publications proposing algorithms for computational efficiency, it has been shown that a combination of even a few of these functions is capable of producing superior SoC estimation methods [60] compared to present simpler approaches. Besides these complex approaches, some effective strategies have been proposed relatively recently to minimize errors produced by simple methods using a sliding mode observer in batteries for hybrid electric vehicles [61].

The high sensitivity of EIS makes it an extremely useful tool for measuring the SoC and state-of-health of batteries [46] and it is likely to be suitable for adaptation into ZBB systems. Regardless of the specific method employed, whether under constant current (galvanostatic) or constant potential (potentiostatic at open-circuit or non-zero potential with respect to a reference electrode), the basis of EIS as a tool for tracking SoC relies on interpreting changes in impedance spectra. Based on currently available literature, the use of EIS in monitoring SoC is primarily limited to Li-ion cells, with some studies also covering lead/acid batteries and nickel-based systems [45, 46]. A primary strategy to measure the low impedance prevalent in batteries is to run impedance tests under the galvanostatic mode, with characteristic inductive loops at particular frequencies and marked changes observed in the low frequency range (≤ 1 Hz) for lead/acid cells [45, 62, 63]. This makes sense, because the longer a battery's charge duration, the higher the degree of depletion of ions involved in redox processes at the respective electrodes, which would in turn lead to impedance contributions attributed to Warburg diffusion limitations observed at lower frequencies. By extension, it is possible that some of these principles could be applied when studying the aqueous-based Zn/Br RFB.

Characteristic resonance frequencies have been noted for Ni/Cd and NiMH cells where the impedance shifts from inductive to capacitive behavior as a function of SoC [64]. This is an interesting and potentially useful phenomenon that could be utilized when adapting EIS for use in ZBB systems. However, the fact remains that EIS by itself contains too many variables and many possibly valid interpretations of impedance spectra. Further studies involving lead/acid batteries have confirmed the usefulness of EIS in determining SoC and state-of-health, but with the important caveat that the information obtained can only be considered reliable if combined with self-learning tools and/or additional algorithms [65]. Combining the sensitivity of EIS with fuzzy logic has been shown to further improve accuracy in determining SoC [66].

2.7 Maximizing Practical Specific Energy of the System

Although there are many conventional and innovative methods of determining SoC, a concurrent main objective should be to achieve maximum utility of the electrolyte's energy capacity. Surprisingly, this important issue is not discussed in the literature despite having direct bearing on the time it takes to charge a Zn/Br RFB and on the practical specific energy of the system. Therefore the issue is briefly highlighted here. Under ideal conditions, the entire stock of primary ions in the primary ZnBr_2 electrolyte should be involved in charge-transfer reactions at the electrodes in order to obtain full utility from a given amount of electrolyte solution. Unfortunately, due to the aqueous nature of the electrolyte solution, practical limitations on the charging and discharging durations of the battery exist in normal operation.

Since the Zn/Br RFB relies on the transport of ions to and from the electrode surfaces, some Zn^{2+} and Br^- ions would still remain in solution after charging has progressed for an extended period of time, with their concentrations reduced to low levels. This situation makes it impractical to continue charging, due to low diffusion rates that would produce only small increments in SoC, meaning that full depletion of the electrolyte is inefficient. Consequently, even if 70 % maximum SoC is reached, 30 % of the capacity is still not utilized despite being physically available. Thus there is an imperative for future designs to seek out methods to increase the practically attainable maximum SoC.

2.8 Moving from Bench Scale to Large/Utility Scale

Migration from developing and testing the new generation of ZBBs from bench to utility-scale operation poses a number of challenges that must be addressed for the technology to be commercially competitive. Factors that will be of prime concern include the purity of electrolyte obtained, as contaminants at even parts-per-million concentrations might result in hydrogen generation, accelerated degradation of

electrode performance or poisoning of the electrolyte solution. Similarly, the quality of electrodes used would influence the rate at which the cell stack requires replacement, thereby directly affecting the maintenance and operating costs of the utility-scale system.

Cell architecture is an important factor influencing flow battery performance. Challenges include design considerations to minimize pumping losses during construction of large-scale systems. An issue unique to flow batteries is the presence of shunt currents. These currents arise through electrical pathways formed through the flow channels feeding each cell. The individual cells are electrically connected in series; however, the electrolyte flows through a manifold in parallel, thereby allowing current to flow between cells through the electrolyte. In practice, this effect is minimized through the use of narrow channels for electrolyte delivery.

Emerging technologies such as 3D-printing are already being investigated [67] and seem to hold much promise for constructing the next-generation of RFB systems, and flexible Zn/Br RFBs have also recently been developed and tested [68]. Furthermore, the final operating environment needs to be given due consideration, with such considerations as suitable heating/cooling strategies to control battery temperatures and achieve optimal operating efficiencies. It is clear that optimizing the system at bench-scale using intelligent materials and predictive control is an appropriate strategy to reduce sources of inefficiencies prior to scale-up. Other challenges, such as power conversion and matching to fluctuations in charging sources and applied loads, will also need to be addressed.

References

1. Cathro KJ (1986) Zinc-bromine batteries for energy storage applications: volume 541 of end of grant report. Department of Resources and Energy, Canberra, Australia
2. Putt RA (1979) Assessment of technical and economic feasibility of zinc/bromine batteries for utility load leveling. Palo Alto, California
3. Cedzynska K (1995) Properties of modified electrolyte for zinc-bromine cells. *Electrochim Acta* 40:971–976. doi:[10.1016/0013-4686\(94\)00372-8](https://doi.org/10.1016/0013-4686(94)00372-8)
4. Cathro KJ, Cedzynska K, Constable DC, Hoobin PM (1986) Selection of quaternary ammonium bromides for use in zinc/bromine cells. *J Power Sources* 18:349–370. doi:[10.1016/0378-7753\(86\)80091-X](https://doi.org/10.1016/0378-7753(86)80091-X)
5. Cathro KJ (1988) Performance of zinc/bromine cells having a propionitrile electrolyte. *J Power Sources* 23:365–383. doi:[10.1016/0378-7753\(88\)80081-8](https://doi.org/10.1016/0378-7753(88)80081-8)
6. Singh P (1984) Application of non-aqueous solvents to batteries. *J Power Sources* 11: 135–142. doi:[10.1016/0378-7753\(84\)80079-8](https://doi.org/10.1016/0378-7753(84)80079-8)
7. Singh P, White K, Parker AJ (1983) Application of non-aqueous solvents to batteries part I. Physicochemical properties of propionitrile/water two-phase solvent relevant to zinc—bromine. *J Power Sources* 10:309–318. doi:[10.1016/0378-7753\(83\)80013-5](https://doi.org/10.1016/0378-7753(83)80013-5)
8. Ponce de Leon C, Walsh FC (2009) Secondary batteries - zinc systems| zinc-bromine. In: Dyer C, Garche J, Moseley P et al (eds) *Encyclopedia of electrochemical power sources*. Elsevier, Amsterdam, pp 487–496
9. Lancry E, Magnes B-Z, Ben-David I, Freiberg M (2013) New bromine complexing agents for bromide based batteries. *ECS Trans* 53:107–115. doi:[10.1149/05307.0107ecst](https://doi.org/10.1149/05307.0107ecst)

10. Blöchl PE (1994) Projector augmented-wave method. *Phys Rev B* 50:17953–17979. doi:[10.1103/PhysRevB.50.17953](https://doi.org/10.1103/PhysRevB.50.17953)
11. Kresse G (1999) From ultrasoft pseudopotentials to the projector augmented-wave method. *Phys Rev B* 59:1758–1775. doi:[10.1103/PhysRevB.59.1758](https://doi.org/10.1103/PhysRevB.59.1758)
12. Kresse G, Furthmüller J (1996) Efficient iterative schemes for ab initio total-energy calculations using a plane-wave basis set. *Phys Rev B: Condens Matter* 54:11169–11186
13. Clark N, Eidler P, Lex P (1999) Development of zinc/bromine batteries for load-leveling applications: phase 2 final report (Sandia Report SAND99-2691). Albuquerque, New Mexico and Livermore, California
14. Linden D, Reddy TB (2001) Handbook of batteries, 3rd edn. McGraw-Hill Professional, New York
15. Baik DS, Fray DJ (2001) Electrodeposition of zinc from high acid zinc chloride solutions. *J Appl Electrochem* 31:1141–1147. doi:[10.1023/A:1012290132379](https://doi.org/10.1023/A:1012290132379)
16. Haller H, Riedel S (2014) Recent discoveries of polyhalogen anions - from bromine to fluorine. *Zeitschrift für anorganische und allgemeine Chemie* 640:1281–1291. doi:[10.1002/zaac.201400085](https://doi.org/10.1002/zaac.201400085)
17. Mader MJ (1986) A mathematical model of a Zn/Br 2 cell on charge. *J Electrochem Soc* 133:1297. doi:[10.1149/1.2108857](https://doi.org/10.1149/1.2108857)
18. Sigma-Aldrich (2014) Material safety data sheet - bromine. Castle Hill, Sydney
19. Yang S-C (1994) An approximate model for estimating the faradaic efficiency loss in zinc/bromine batteries caused by cell self-discharge. *J Power Sources* 50:343–360. doi:[10.1016/0378-7753\(94\)01910-X](https://doi.org/10.1016/0378-7753(94)01910-X)
20. Chiu SL, Selman JR (1992) Determination of electrode kinetics by corrosion potential measurements: zinc corrosion by bromine. *J Appl Electrochem* 22:28–37. doi:[10.1007/BF01093008](https://doi.org/10.1007/BF01093008)
21. Lim HS (1977) Zinc-bromine secondary battery. *J Electrochem Soc* 124:1154–1157. doi:[10.1149/1.2133517](https://doi.org/10.1149/1.2133517)
22. Heintz A, Illenberger C (1996) Diffusion coefficients of Br 2 in cation exchange membranes. *J Membr Sci* 113:175–181. doi:[10.1016/0376-7388\(95\)00026-7](https://doi.org/10.1016/0376-7388(95)00026-7)
23. Cathro KJ, Constable DC, Hoobin PM (1988) Performance of porous plastic separators in zinc/bromine cells. *J Power Sources* 22:29–57. doi:[10.1016/0378-7753\(88\)80004-1](https://doi.org/10.1016/0378-7753(88)80004-1)
24. Bellows RJ, Grimes P, Einstein H et al (1983) Zinc-bromine battery design for electric vehicles. *IEEE Trans Veh Technol* 32:26–32. doi:[10.1109/T-VT.1983.23941](https://doi.org/10.1109/T-VT.1983.23941)
25. Eidler P (1999) Development of zinc/bromine batteries for load-leveling applications: phase 1 final report (Sandia Report SAND99-1853). Albuquerque, New Mexico and Livermore, California
26. Will FG (1979) Recent advances in zinc-bromine batteries. In: Proceedings of the eleventh international symposium, 25–28 September 1978. Academic Press, Inc. (London), Ltd., Brighton, Sussex, England, pp 313–326
27. Maurya S, Shin S-H, Kim Y, Moon S-H (2015) A review on recent developments of anion exchange membranes for fuel cells and redox flow batteries. *RSC Adv* 5:37206–37230. doi:[10.1039/C5RA04741B](https://doi.org/10.1039/C5RA04741B)
28. Gu S, Gong K, Yan EZ, Yan Y (2014) A multiple ion-exchange membrane design for redox flow batteries. *Energy Environ Sci* 7:2986. doi:[10.1039/C4EE00165F](https://doi.org/10.1039/C4EE00165F)
29. Arnold C, Assink RA (1988) Development of sulfonated polysulfone membranes for redox flow batteries. *J Membr Sci* 38:71–83. doi:[10.1016/S0376-7388\(00\)83276-7](https://doi.org/10.1016/S0376-7388(00)83276-7)
30. Hinkle KR, Jameson CJ, Murad S (2014) Transport of Vanadium and Oxovanadium Ions Across Zeolite Membranes: A Molecular. *J Phys Chem C* 118:23803–23810. doi:[10.1021/jp507155s](https://doi.org/10.1021/jp507155s)
31. Xiangguo T, Jicui D, Jing S (2014) Effects of different kinds of surfactants on Nafion membranes for all vanadium redox flow battery. *J Solid State Electrochem*. doi:[10.1007/s10008-014-2713-7](https://doi.org/10.1007/s10008-014-2713-7)
32. Winardi S, Poon G, Ulaganathan M et al (2015) Effect of bromine complexing agents on the performance of cation exchange membranes in second-generation vanadium bromide battery. *ChemPlusChem* 80:376–381. doi:[10.1002/cplu.201402260](https://doi.org/10.1002/cplu.201402260)

33. Pop V, Bergveld HJ, Danilov D, et al. (2008) Battery management systems: accurate state-of-charge indication for battery-powered applications. Philips research book series, vol 9. Springer Science + Business Media B.V, London
34. Piller S, Perrin M, Jossen A (2001) Methods for state-of-charge determination and their applications. *J Power Sources* 96:113–120. doi:[10.1016/S0378-7753\(01\)00560-2](https://doi.org/10.1016/S0378-7753(01)00560-2)
35. Pang S, Farrell J, Du J, Barth M (2001) Battery state-of-charge estimation. In: Proceedings of the 2001 American control conference. (Cat. No.01CH37148), pp 1644–1649. IEEE, Arlington
36. Ng KS, Moo C-S, Chen Y-P, Hsieh Y-C (2009) Enhanced coulomb counting method for estimating state-of-charge and state-of-health of lithium-ion batteries. *Appl Energy* 86:1506–1511. doi:[10.1016/j.apenergy.2008.11.021](https://doi.org/10.1016/j.apenergy.2008.11.021)
37. Lukic SM, Bansal RC, Rodriguez F, Emadi A (2008) Energy Storage Syst Automot Appl. *IEEE Trans Industr Electron* 55:2258–2267. doi:[10.1109/TIE.2008.918390](https://doi.org/10.1109/TIE.2008.918390)
38. Bhangu BS, Bentley P, Stone DA, Bingham CM (2005) Nonlinear observers for predicting state-of-charge and state-of-health of lead-acid batteries for hybrid-electric vehicles. *IEEE Trans Veh Technol* 54:783–794. doi:[10.1109/TVT.2004.842461](https://doi.org/10.1109/TVT.2004.842461)
39. Vasebi A, Partovibakhsh M, Bathaee SMT (2007) A novel combined battery model for state-of-charge estimation in lead-acid batteries based on extended Kalman filter for hybrid electric vehicle applications. *J Power Sources* 174:30–40. doi:[10.1016/j.jpowsour.2007.04.011](https://doi.org/10.1016/j.jpowsour.2007.04.011)
40. Vasebi A, Bathaee SMT, Partovibakhsh M (2008) Predicting state of charge of lead-acid batteries for hybrid electric vehicles by extended Kalman filter. *Energy Convers Manag* 49:75–82. doi:[10.1016/j.enconman.2007.05.017](https://doi.org/10.1016/j.enconman.2007.05.017)
41. Santhanagopalan S, White RE (2006) Online estimation of the state of charge of a lithium ion cell. *J Power Sources* 161:1346–1355. doi:[10.1016/j.jpowsour.2006.04.146](https://doi.org/10.1016/j.jpowsour.2006.04.146)
42. Plett GL (2004) Extended Kalman filtering for battery management systems of LiPB-based HEV battery packs. *J Power Sources* 134:277–292. doi:[10.1016/j.jpowsour.2004.02.033](https://doi.org/10.1016/j.jpowsour.2004.02.033)
43. Lee S, Kim J, Lee J, Cho BH (2008) State-of-charge and capacity estimation of lithium-ion battery using a new open-circuit voltage versus state-of-charge. *J Power Sources* 185:1367–1373. doi:[10.1016/j.jpowsour.2008.08.103](https://doi.org/10.1016/j.jpowsour.2008.08.103)
44. Skyllas-Kazacos M, Kazacos M (2011) State of charge monitoring methods for vanadium redox flow battery control. *J Power Sources* 196:8822–8827. doi:[10.1016/j.jpowsour.2011.06.080](https://doi.org/10.1016/j.jpowsour.2011.06.080)
45. Rodrigues S, Munichandraiah N, Shukla AK (2000) A review of state-of-charge indication of batteries by means of a.c. impedance measurements. *J Power Sources* 87:12–20. doi:[10.1016/S0378-7753\(99\)00351-1](https://doi.org/10.1016/S0378-7753(99)00351-1)
46. Huet F (1998) A review of impedance measurements for determination of the state-of-charge or state-of-health of secondary batteries. *J Power Sources* 70:59–69. doi:[10.1016/S0378-7753\(97\)02665-7](https://doi.org/10.1016/S0378-7753(97)02665-7)
47. Thele M, Bohlen O, Sauer DU, Karden E (2008) Development of a voltage-behavior model for NiMH batteries using an impedance-based modeling concept. *J Power Sources* 175:635–643. doi:[10.1016/j.jpowsour.2007.08.039](https://doi.org/10.1016/j.jpowsour.2007.08.039)
48. Sabatier J, Aoun M, Oustaloup A et al (2006) Fractional system identification for lead acid battery state of charge estimation. *Sig Process* 86:2645–2657. doi:[10.1016/j.sigpro.2006.02.030](https://doi.org/10.1016/j.sigpro.2006.02.030)
49. Takano K, Nozaki K, Saito Y et al (2000) Impedance spectroscopy by voltage-step chronoamperometry using the Laplace transform method in a lithium-ion battery. *J Electrochem Soc* 147:922–929. doi:[10.1149/1.1393293](https://doi.org/10.1149/1.1393293)
50. Delaille A, Perrin M, Huet F, Hernout L (2006) Study of the “coup de fouet” of lead-acid cells as a function of their state-of-charge and state-of-health. *J Power Sources* 158:1019–1028. doi:[10.1016/j.jpowsour.2005.11.015](https://doi.org/10.1016/j.jpowsour.2005.11.015)
51. Verbrugge M, Tate E (2004) Adaptive state of charge algorithm for nickel metal hydride batteries including hysteresis phenomena. *J Power Sources* 126:236–249. doi:[10.1016/j.jpowsour.2003.08.042](https://doi.org/10.1016/j.jpowsour.2003.08.042)

52. Rong P, Pedram M (2006) An analytical model for predicting the remaining battery capacity of lithium-ion batteries. *IEEE Trans Very Large Scale Integr VLSI Syst* 14:441–451. doi:[10.1109/TVLSI.2006.876094](https://doi.org/10.1109/TVLSI.2006.876094)
53. Shen Y (2010) Adaptive online state-of-charge determination based on neuro-controller and neural network. *Energy Convers Manag* 51:1093–1098. doi:[10.1016/j.enconman.2009.12.015](https://doi.org/10.1016/j.enconman.2009.12.015)
54. Cai C, Du D, Liu Z, Ge J (2002) State-of-charge (SOC) estimation of high power Ni-MH rechargeable battery with artificial neural network. In: *Proceedings of the 9th international conference on neural information processing, ICONIP '02*, pp 824–828. Nanyang Technol. Univ
55. Grewal S, Grant DA (2001) A novel technique for modelling the state of charge of lithium ion batteries using artificial neural networks. *Twenty-Third International Telecommunications Energy Conference. INTELEC 2001. IEE*, pp 174–179
56. Singh P, Vinjamuri R, Wang X, Reisner D (2006) Design and implementation of a fuzzy logic-based state-of-charge meter for Li-ion batteries used in portable defibrillators. *J Power Sources* 162:829–836. doi:[10.1016/j.jpowsour.2005.04.039](https://doi.org/10.1016/j.jpowsour.2005.04.039)
57. Salkind AJ, Fennie C, Singh P et al (1999) Determination of state-of-charge and state-of-health of batteries by fuzzy logic methodology. *J Power Sources* 80:293–300. doi:[10.1016/S0378-7753\(99\)00079-8](https://doi.org/10.1016/S0378-7753(99)00079-8)
58. Lee D-T, Shiah S-J, Lee C-M, Wang Y-C (2007) State-of-charge estimation for electric scooters by using learning mechanisms. *IEEE Trans Veh Technol* 56:544–556. doi:[10.1109/TVT.2007.891433](https://doi.org/10.1109/TVT.2007.891433)
59. Cai CH, Du D, Liu ZY (2003) Battery state-of-charge (SOC) estimation using adaptive neuro-fuzzy inference system (ANFIS). In: *Proceedings of the 12th IEEE international conference on fuzzy systems, FUZZ'03*, pp 1068–1073. IEEE
60. Lee Y, Wang W, Kuo T (2008) Soft Computing for Battery State-of-Charge (BSOC) Estimation in Battery String Systems. *IEEE Trans Industr Electron* 55:229–239. doi:[10.1109/TIE.2007.896496](https://doi.org/10.1109/TIE.2007.896496)
61. Kim I (2008) Nonlinear state of charge estimator for hybrid electric vehicle battery. *IEEE Trans Power Electron* 23:2027–2034. doi:[10.1109/TPEL.2008.924629](https://doi.org/10.1109/TPEL.2008.924629)
62. Viswanathan VV, Salkind AJ, Kelley JJ, Ockerman JB (1995) Effect of state of charge on impedance spectrum of sealed cells Part II: Lead acid batteries. *Journal of Applied Electrochemistry* 25:729–739. doi:[10.1007/BF00648628](https://doi.org/10.1007/BF00648628)
63. Gopikanth ML, Sathyanarayana S (1979) Impedance parameters and the state-of-charge. II. lead-acid battery. *J Appl Electrochem* 9:369–379. doi:[10.1007/BF01112492](https://doi.org/10.1007/BF01112492)
64. Hammouche A, Karden E, De Doncker RW (2004) Monitoring state-of-charge of Ni–MH and Ni–Cd batteries using impedance spectroscopy. *J Power Sources* 127:105–111. doi:[10.1016/j.jpowsour.2003.09.012](https://doi.org/10.1016/j.jpowsour.2003.09.012)
65. Blanke H, Bohlen O, Buller S et al (2005) Impedance measurements on lead–acid batteries for state-of-charge, state-of-health and cranking capability prognosis in electric and hybrid electric vehicles. *J Power Sources* 144:418–425. doi:[10.1016/j.jpowsour.2004.10.028](https://doi.org/10.1016/j.jpowsour.2004.10.028)
66. Singh P, Fennie C, Reisner DE, Salkind A (2000) Fuzzy logic enhanced electrochemical impedance spectroscopy (FLEEIS) to determine battery state-of-charge. In: *Proceedings of the 15th annual battery conference on applications and advances*, pp 199–204. Long Beach, 11–14 January 2000
67. Arenas LF, Walsh FC, de Leon CP (2015) 3D-printing of redox flow batteries for energy storage: a rapid prototype laboratory cell. *ECS J Solid State Sci Technol* 4:P3080–P3085. doi:[10.1149/2.0141504jss](https://doi.org/10.1149/2.0141504jss)
68. Peng M, Yan K, Hu H et al (2015) Efficient fiber shaped zinc bromide batteries and dye sensitized solar cells for flexible power sources. *J Mater Chem C* 3:2157–2165. doi:[10.1039/C4TC02997F](https://doi.org/10.1039/C4TC02997F)

The Zinc/Bromine Flow Battery

Materials Challenges and Practical Solutions for
Technology Advancement

Rajaratnam, G.P.; Vassallo, A.M.

2016, XXI, 97 p. 31 illus., 26 illus. in color., Softcover

ISBN: 978-981-287-645-4